Electronic Supplementary Material (ESI) for Nanoscale.

Supporting information for:

Langmuir and Langmuir-Blodgett technologies as nanoarchitectonic tools for the incorporation of curcumin in membrane systems

Laura Dotor, José Miguel García-Pinilla, Santiago Martín, Pilar Cea*

Instituto de Nanociencia y Materiales de Aragón (INMA), CSIC-Universidad de Zaragoza, 50009 Zaragoza, Spain.
Laboratorio de Microscopias Avanzadas (LMA), Universidad de Zaragoza, 50018, Zaragoza, Spain.
Departamento de Química Física, Facultad de Ciencias, Universidad de Zaragoza, 50009 Zaragoza, Spain.

***Corresponding author**
e-mail address: pilarcea@unizar.es

Table of Contents for the Supporting Information

Section S1. Discussion for the DPPC and CHOL isotherms and their mixtures

For the DPPC monolayer, the lift-off in the π-*A* isotherm occurs at ca. 1.09 $nm^2 \cdot molecule^{-1}$ (Figure 2.a in the paper); this area per molecule denotes the first value at which the surface pressure can be detected upon the compression process, i.e. $\pi \cong 0.5$ $mN \cdot m^{-1}$, and it corresponds to the transition from a G to LE phase. The change of slope at 5-10 $mN \cdot m^{-1}$ is indicative of a phase transition between the LE and LC phases. The K_s-π plot (Figure 2.b) indicates that the LC phase is reached at ca. π = 15 $mN \cdot m^{-1}$ and the monolayer remains in that state till the collapse occurs at π = 67 $mN \cdot m^{-1}$ (with a maximum K_s value of 247 $mN \cdot m^{-1}$, which is very close to the limit between LC-S phases). The collapse surface pressure was determined by projection on the y-axis (π) of the intersection point of the two lines being extensions of the isotherm below and above its inflection (collapse). The surface behaviour for DPPC can be explained taking into account that this molecule is a lipid composed by a polar phosphatidylcholine group and two nonpolar palmitic acid (C_{16}) chains. The acceptors atoms of the polar head lead to hydrogen bonding, while the saturated bonds of the tails promote chain order by means of lateral van der Waals interactions. At the same time, the extremely high number of rotatable bonds provokes a high conformational flexibility. In fact, DPPC remains in a LC phase without reaching a S phase. With regard to the CHOL monolayer, the lift-off in the isotherm occurs at ca. 0.36 $nm^2 \cdot molecule^{-1}$ (Figure 2.a). Beyond this point, the surface pressure increases monotonously until the collapse is reached at 46 $mN \cdot m^{-1}$. In the K_s-π plot (Figure 2.b), the transition between LE-LC phases can be noticed at a very low surface pressure, ca. π = 2 $mN \cdot m^{-1}$, and the transition between LC-S phases occurs at ca. π = 8 $mN \cdot m^{-1}$. The maximum K_s value reached for CHOL is 469 $mN \cdot m^{-1}$. In other words, CHOL features a more condensed monolayer than DPPC. Such a behavior can be also explained in terms of the chemical structure of CHOL that contains a sterane structure (cyclopentanoperhydrophenanthrenes) with a hydroxyl group in C3. Since CHOL is in a trans conformation, all but the side chain is rigid and planar, leading to close-packed monolayers.

The binary mixtures of DPPC and CHOL have also been studied in this work for an extensive comparison with the binary mixtures of DPPC+CCM and DPPC+CHOL under the same experimental conditions, section S3, and later the ternary mixtures DPPC+CHOL+CMM, section S4. Figure S1 shows the π-A isotherms for (DPPC+CHOL) in the whole range of molar fractions together with the K_s values for this binary system. CHOL exhibits a condensation effect on DPPC monolayers (negative excess areas per molecule)[1,2] as a result of DPPC and CHOL interactions, with CHOL decreasing the free volume of the DPPC and ordering the lipid chains.

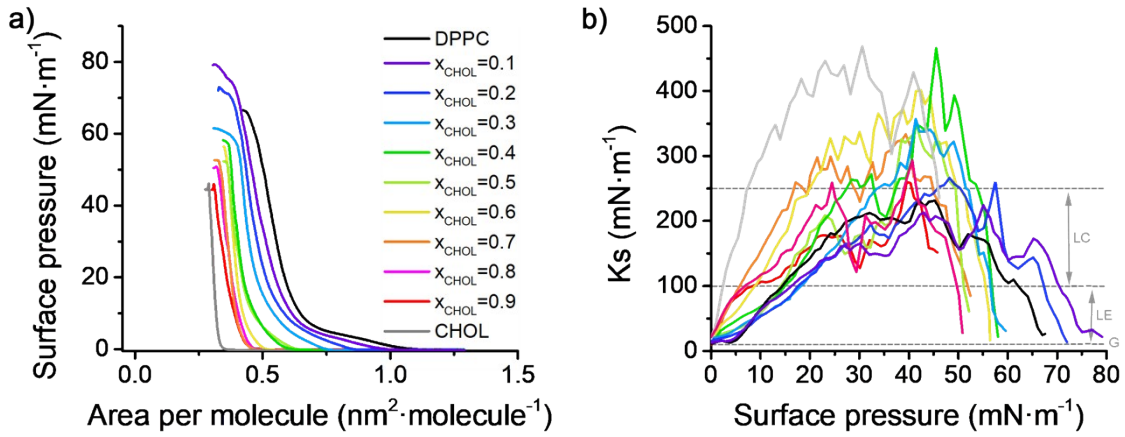

Figure S1. (a) Isotherms for the indicated binary mixtures of DPPC and CHOL and (b) K_s values for these Langmuir films.

Section S2. Discussion for the CCM stability at the air-water interface

The stability of CCM has been studied at the air water interface. Fist, the loss of the area per molecule at a target surface pressure of 30 mN·m^{-1}, Figure S2, was determined. A significant decrease in the area per molecule is observed. The result is in agreement with a liquid expanded phase (see Figure 2 in the paper) despite the relatively high surface pressure, since the monolayer is in a fluid phase.

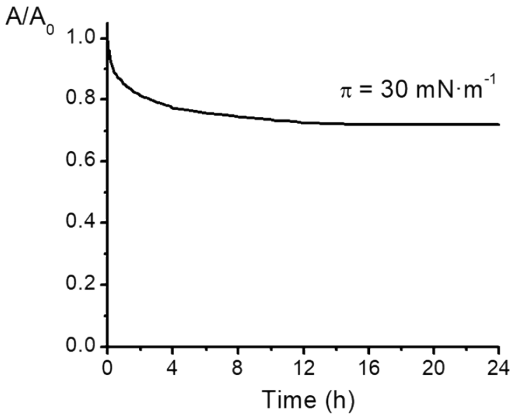

Figure S2. Reduction in the area per molecule for a CCM monolayer at the air-water interface maintained at a constant surface pressure of 30 mN·m^{-1}, expressed as the area at the indicated time divided by the area per molecule at which the initial target surface pressure was reached, A_0.

In order to either confirm or rule out a possible loss of molecules towards the subphase, compression-decompression hysteresis cycles were performed. The first cycle is shown in Figure S3. A negligible hysteresis is observed. Additionally, the subsequent cycles follow practically the same trajectory as the first one with only negligible shift towards smaller areas per molecule. These results rule out the loss of molecules towards the subphase but indicate a loosy film at the air-water interface with a continuous reorganization of the molecules

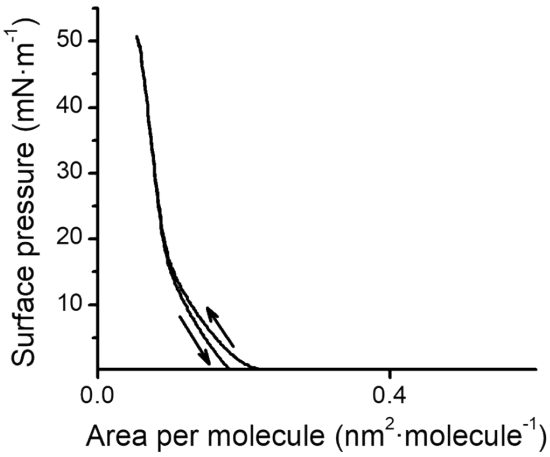

Figure S3. First hysteresis cycle for the compression and decompression of a CCM monolayer at the air-water interface.

Section S3. Thermodynamic study of the binary mixtures

In addition to the (DPPC+CHOL) mixtures (Section S1) the isotherms for the binary mixtures of (DPPC+CCM) and (CHOL+CCM) were recorded, Figure S4. Both DPPC and CHOL have a condensing effect on CCM monolayers, with *Ks* values for the CCM mixtures higher than the pure compound.

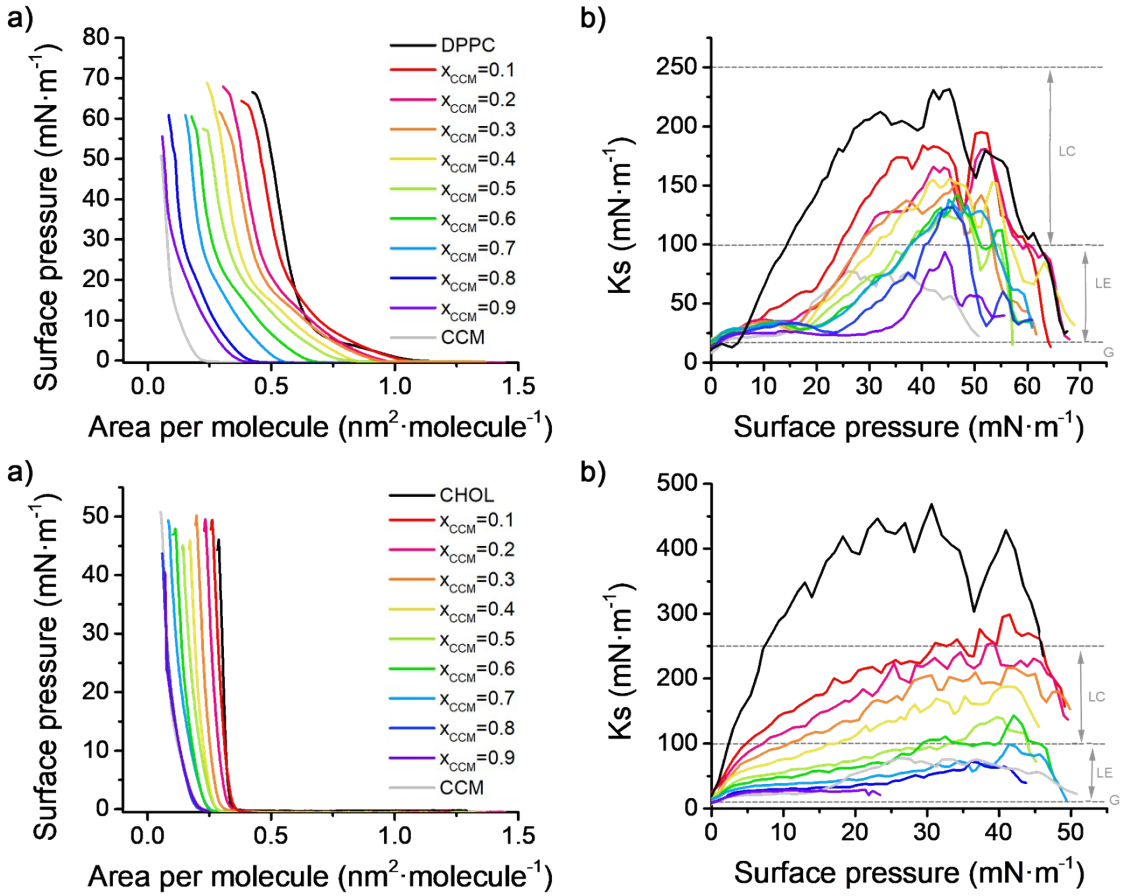

Figure S4. (a) π-*A* isotherms for the (CCM/DPPC), (CCM/CHOL) and (DPPC/CHOL) binary systems at 20 ºC. (b) K_s-π plots the (CCM/DPPC), (CCM/CHOL) and (DPPC/CHOL) binary systems.

In order to discern whether these mixtures are partially miscible or immiscible the collapse surface pressure for the mixed films was recorded and analysed versus the composition, Figure S5. With regard to the collapse surface pressure in the binary (DPPC/CHOL) monolayers, deviations from ideality occur, indicative of partially miscible components in the mixed monolayers, which is in good agreement with previous observations in the literature.[1] In a similar but even more evident manner, DPPC/CCM and CHOL/CCM mixtures also deviate from the ideality with collapse surface pressures above or below the ideal behaviour (dotted line). In addition to the collapse surface pressure, the maximum *Ks* values for the mixed films and also the surface pressures at which these maximum Ks values are reached, were determined and represented versus the molar fraction. These plots are indicative of the mechanical stability of the monolayer (and the surface pressure at which it is reached), because is just before the mechanical destabilization of the monolayer originates by the compression process (including buckling- or weakening – phenomena) that may happen previously to the collapse. CCM induces a fluidization of the monolayer, larger than the ideal mixing value, and also results in larger surface pressures for the maximum *Ks* value in the mixed films.

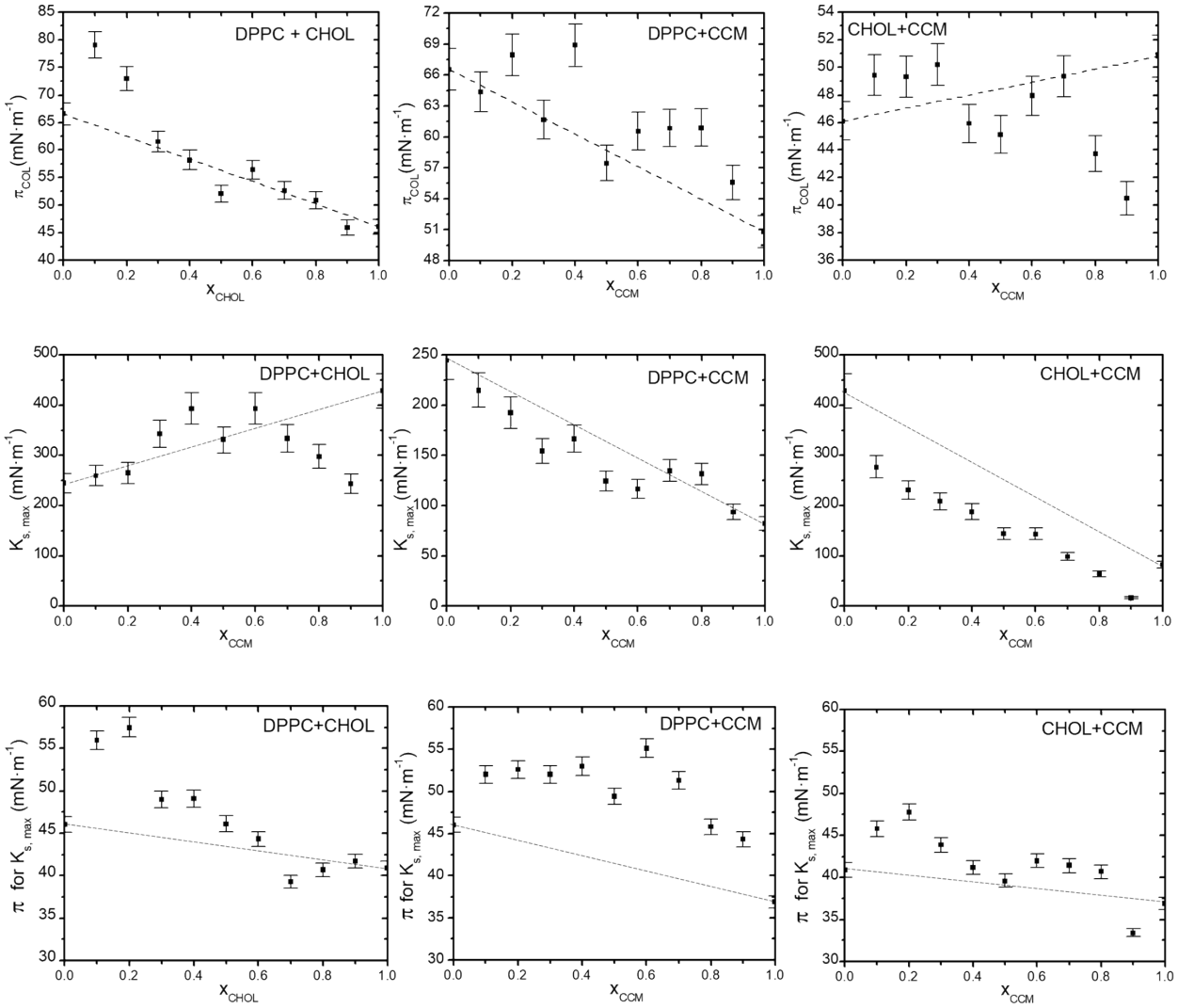

Figure S5. Surface pressures of collapse for the indicated binary mixtures in terms of the composition of the mixture.

Additionally, the *Ks* values for all the binary mixtures here studied have been calculated at several surface pressures of transference, Figure S6. From these figures it can be concluded that CMM induces a larger fluidization of the monolayer in the mixed films than that expected from an ideal mixture

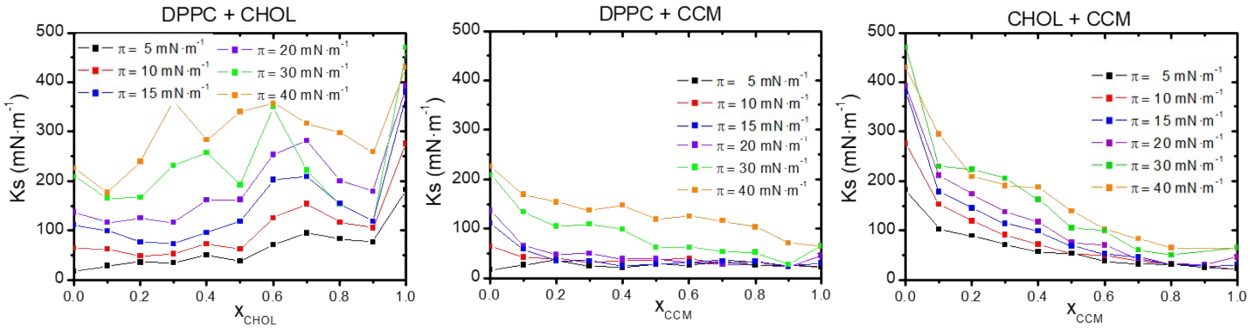

Figure S6. Compression modulus for the indicated binary mixtures in terms of the composition of the mixture.

Figure S7 gathers the excess thermodynamic properties, namely A^E and ΔG_m^E as well as the Gibbs energy of mixing, ΔG_m, for the three binary mixtures here studied. Deviations from the ideality are indicative of immiscible or partially miscible films.

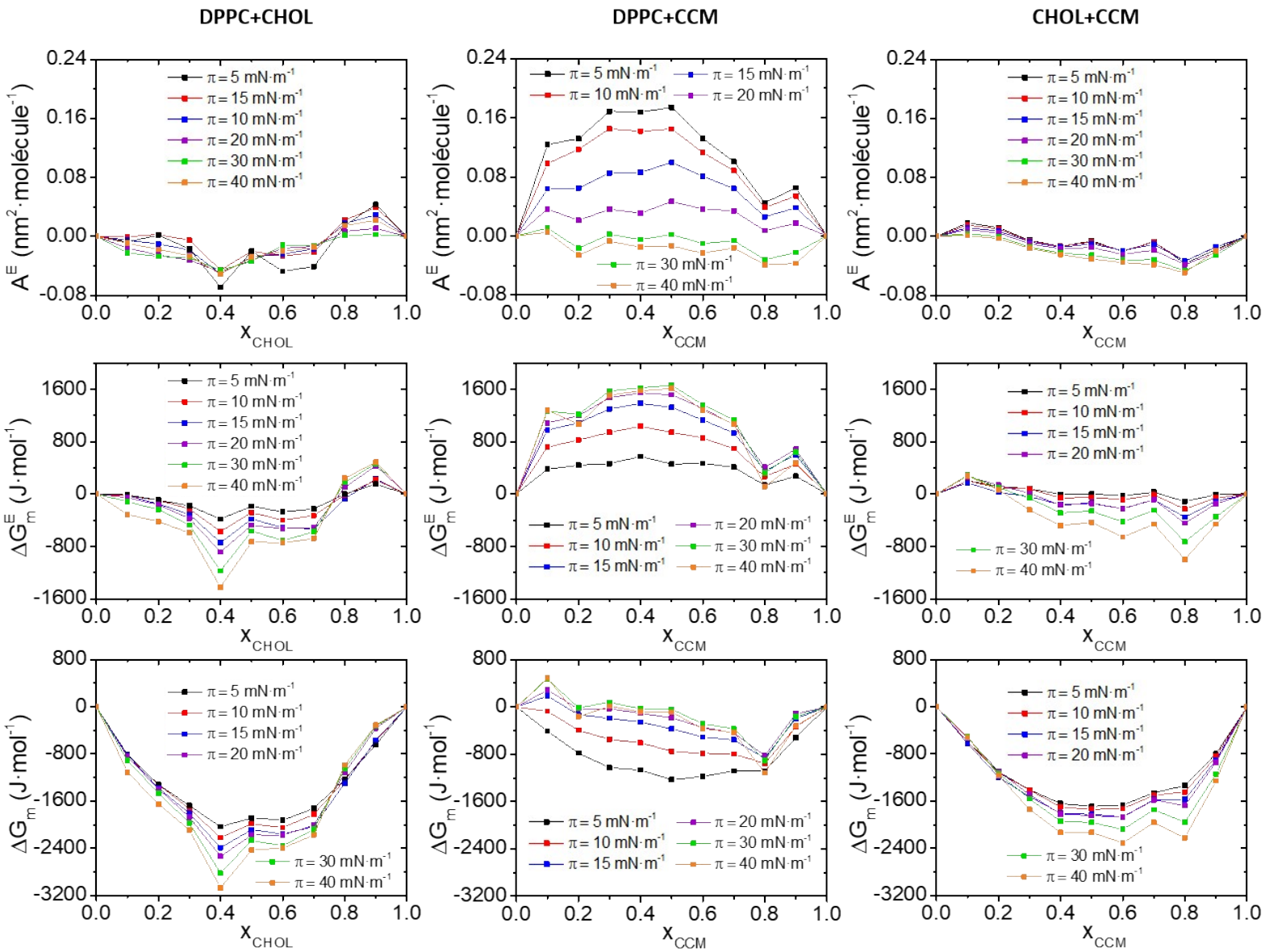

Figure S7. Excess area, A^E, excess Gibbs energy of mixing, ΔG^E_m, and Gibbs energy of mixing, ΔG_m, for the indicated binary mixtures in terms of the composition at the indicated surface pressures.

Section S4. Thermodynamic study of the ternary mixtures at the air-water interface.

Figure S8 shows a ternary diagram exhibiting the compositions that were analysed in this contribution, whilst Figure S9 shows the isotherms recorded for these ternary systems.

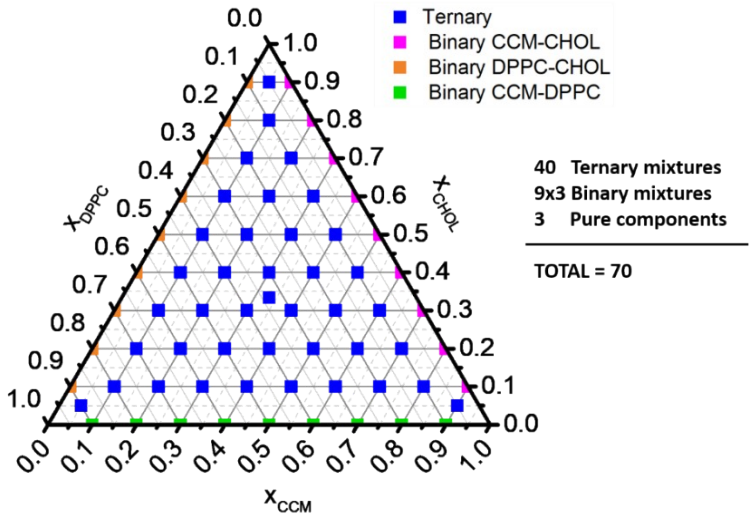

Figure S8. Ternary diagram showing the compositions of the 70 mixtures considered in this work.

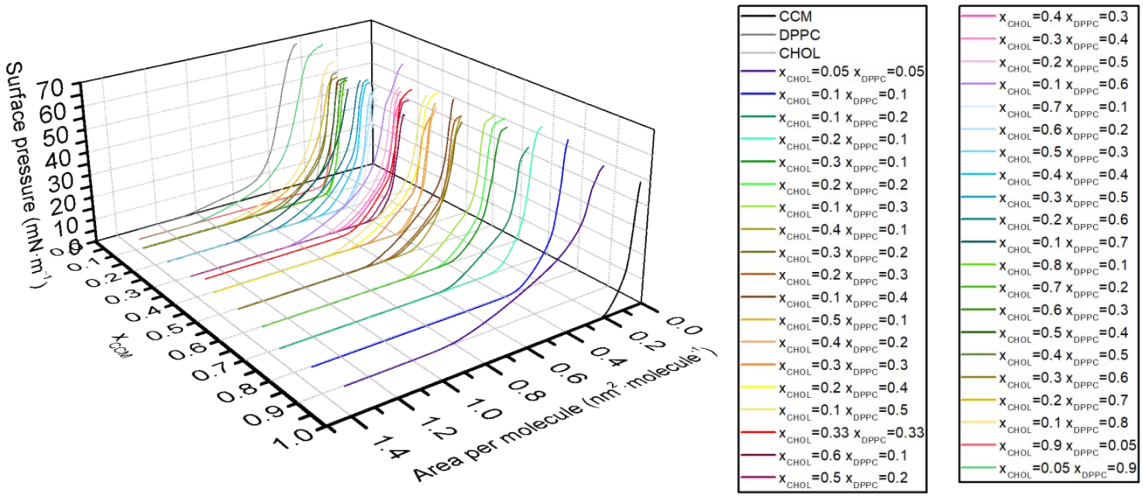

Figure S9.1. π-*A* isotherms for CCM-DPPC-CHOL ternary systems at different molar fractions of CCM**.**

In the following figures, the influence of CHOL and DPPC at the same CCM molar fraction is studied with detailed plots of the surface pressure-area (π-*A*) isotherms.

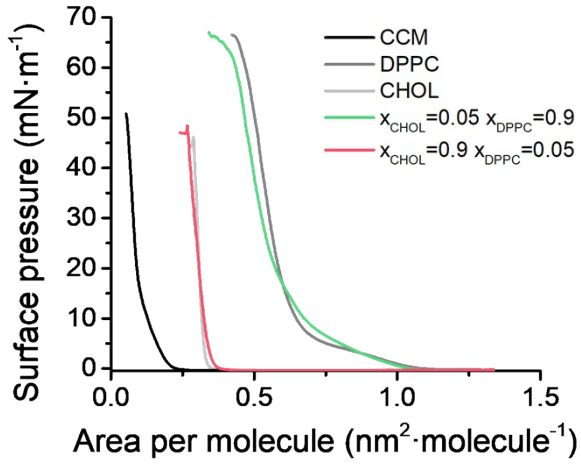

Figure S9.2. π- *A* isotherms for the ternary mixed monolayers with x_{CCM} = 0.05 at 20 ºC.

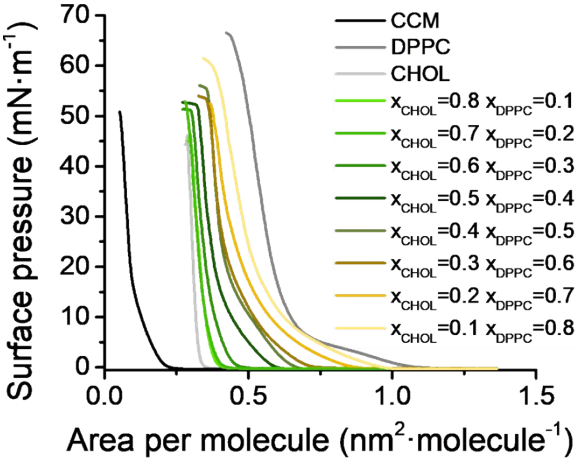

Figure S9.3. π- *A* isotherms for the ternary mixed monolayers with x_{CCM} = 0.1 at 20 ºC.

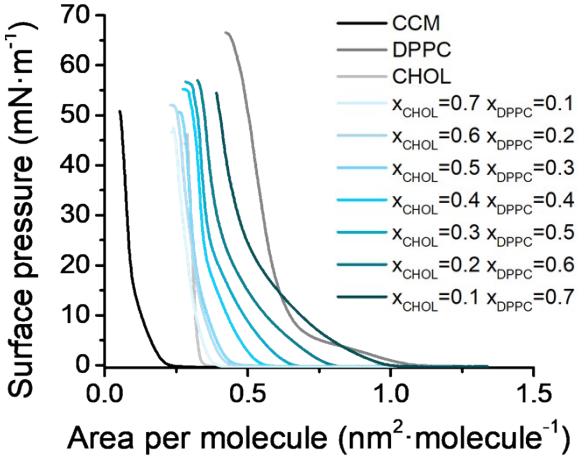

Figure S9.4. π- *A* isotherms for the ternary mixed monolayers with x_{CCM} = 0.2 at 20 ºC.

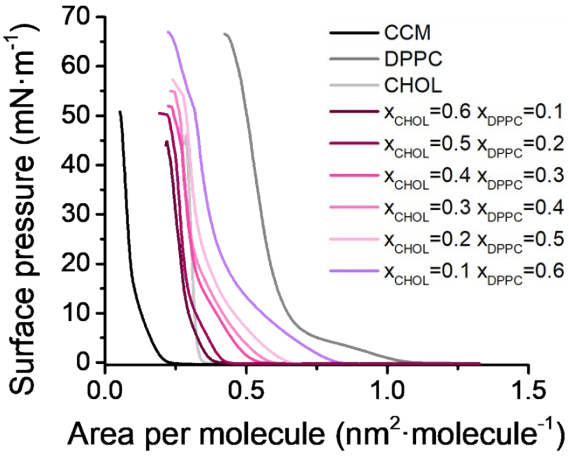

Figure S9.5. π- *A* isotherms for the ternary mixed monolayers with x_{CCM} = 0.3 at 20 ºC.

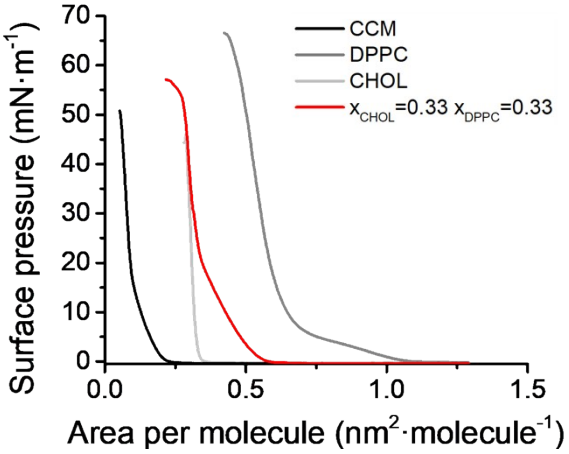

Figure S9.6. π- *A* isotherms for the ternary mixed monolayers with x_{CCM} = 0.33 at 20 ºC.

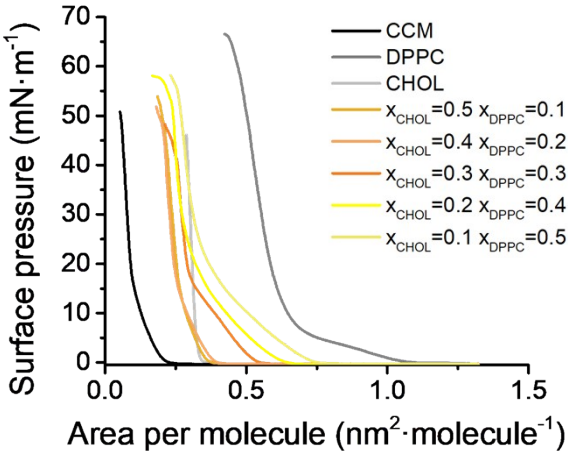

Figure S9.7. π- *A* isotherms for the ternary mixed monolayers with x_{CCM} = 0.4 at 20 ºC.

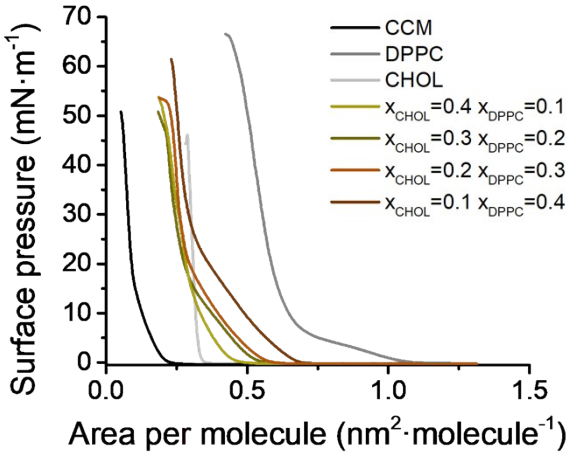

Figure S9.8. π- *A* isotherms for the ternary mixed monolayers with x_{CCM} = 0.5 at 20 ºC.

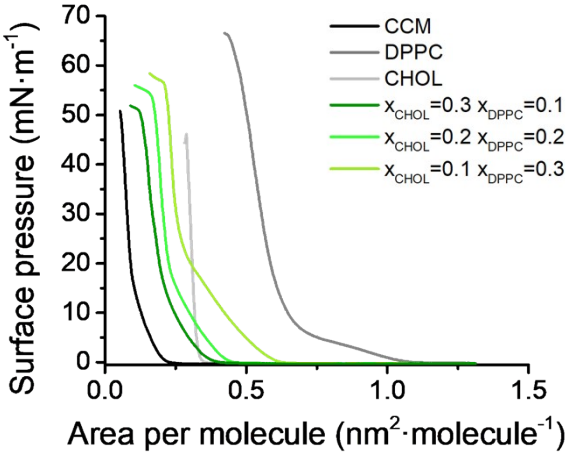

Figure S9.9. π- *A* isotherms for the ternary mixed monolayers with x_{CCM} = 0.6 at 20 ºC.

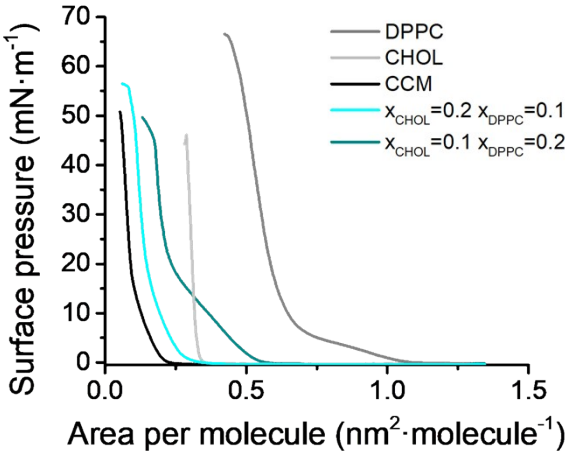

Figure S9.10. π- *A* isotherms for the ternary mixed monolayers with x_{CCM} = 0.7 at 20 ºC.

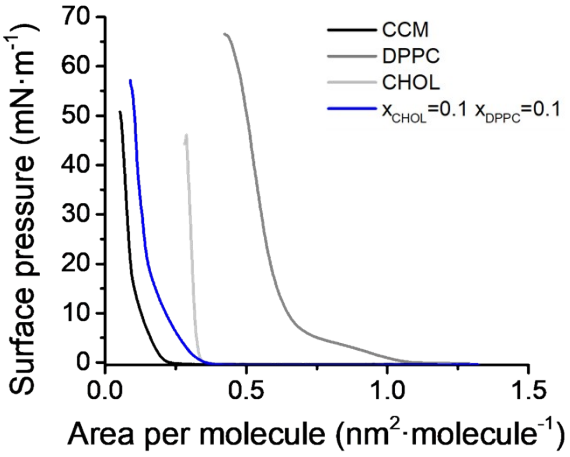

Figure S9.11. π- *A* isotherms for the ternary mixed monolayers with x_{CCM} = 0.8 at 20 ºC.

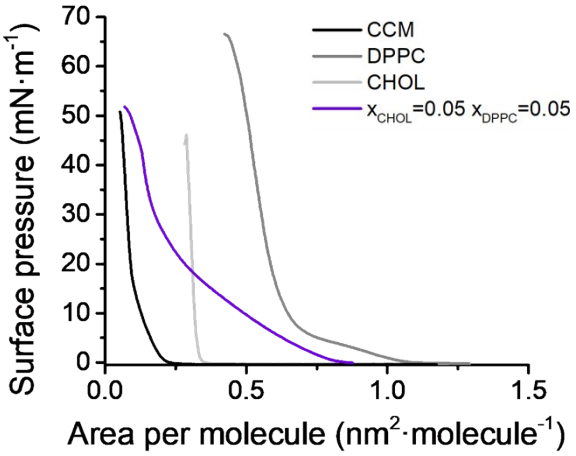

Figure S9.12. π- *A* isotherms for the ternary mixed monolayers with x_{CCM} = 0.9 at 20 ºC.

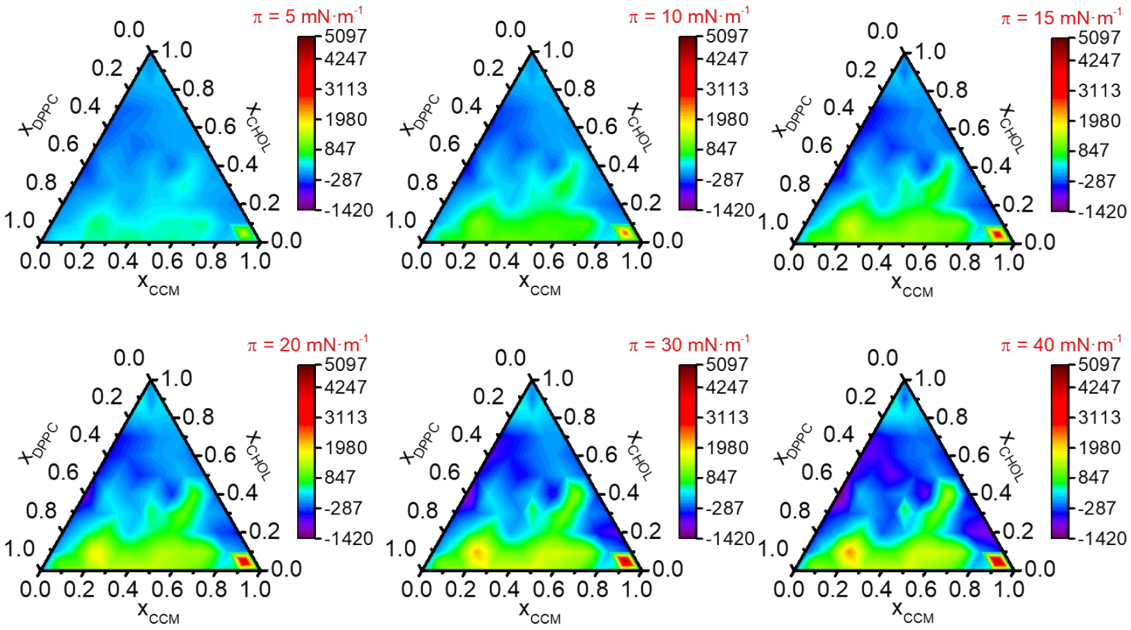

Figure S10. ΔG^E_m expressed in J·mol^{-1} vs. molar fraction in (DPPC+CHOL+CCM) ternary system for the indicated surface pressures.

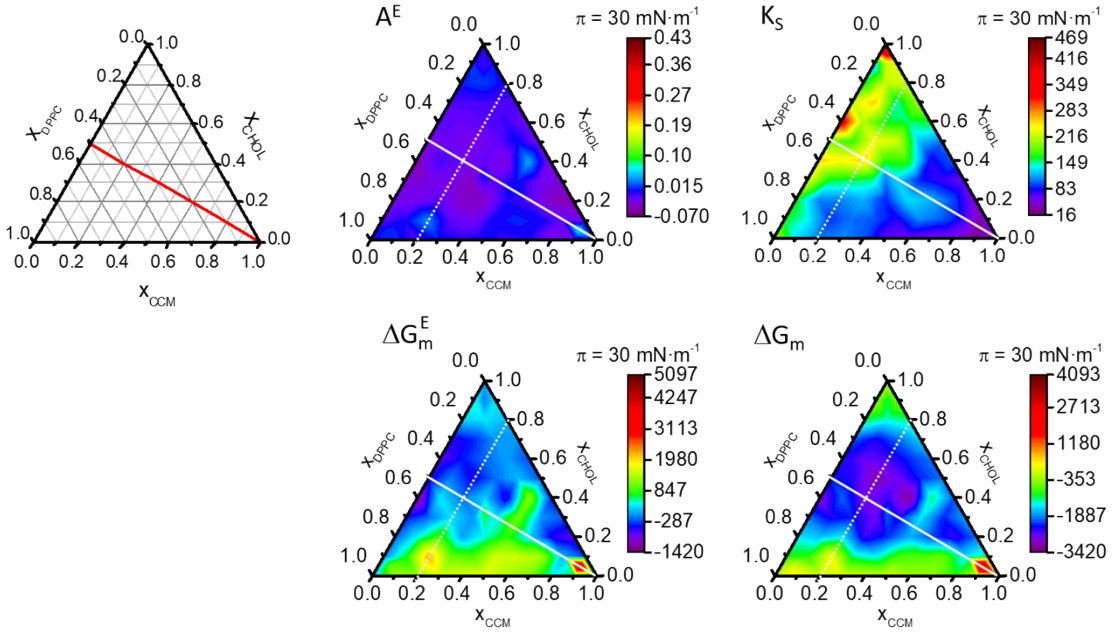

Figure S11. The ternary diagram in the top of the first column contains a red line that indicates the mixtures in which the DDPC/CHOL ratio is maintained constant in the 1/1 proportion. The ternary diagrams in the second and third column correspond to the indicated properties measured at a surface pressure of 30 mN·m^{-1}. The solid white line indicates the points in which the DPPC/CHOL ratio is 1/1 and the dotted white line the points for which the X_{CCM} is 0.2.

Table S.I. Thermodynamic parameters for the mixtures maintaining constant the composition of DPPC/CHOL 1/1 at the whole range of surface pressures.

			A^E (nm²·molecule⁻¹)						K_s (mN·m⁻¹)					
x_{CCM}	x_{CHOL}	x_{DPPC}	5 mN·m⁻¹	10 mN·m⁻¹	15 mN·m⁻¹	20 mN·m⁻¹	30 mN·m⁻¹	40 mN·m⁻¹	5 mN·m⁻¹	10 mN·m⁻¹	15 mN·m⁻¹	20 mN·m⁻¹	30 mN·m⁻¹	40 mN·m⁻¹
0	**0.5**	**0.5**	-0.020	-0.020	-0.028	-0.028	-0.032	-0.034	37	61	118	163	191	340
0.2	**0.4**	**0.4**	0.010	0.017	0.002	-0.015	-0.020	-0.016	45	58	55	76	257	256
0.33	**0.33**	**0.33**	0.067	0.065	0.042	0.018	0.004	0.002	35	44	39	61	113	244
0.4	**0.3**	**0.3**	0.065	0.048	0.004	-0.014	-0.017	-0.017	36	29	30	98	130	131
0.6	**0.2**	**0.2**	0.043	0.029	0.008	-0.008	-0.012	-0.012	24	29	36	69	119	164
0.8	**0.1**	**0.1**	0.027	0.016	0.003	-0.010	-0.018	-0.023	24	27	31	43	75	93
0.9	**0.05**	**0.05**	0.429	0.328	0.237	0.156	0.064	0.034	25	22	16	20	28	48
			ΔG_m^E (J·mol⁻¹)						ΔG_m(J·mol⁻¹)					
x_{CCM}	x_{CHOL}	x_{DPPC}	5 mN·m⁻¹	10 mN·m⁻¹	15 mN·m⁻¹	20 mN·m⁻¹	30 mN·m⁻¹	40 mN·m⁻¹	5 mN·m⁻¹	10 mN·m⁻¹	15 mN·m⁻¹	20 mN·m⁻¹	30 mN·m⁻¹	40 mN·m⁻¹
0	**0.5**	**0.5**	-186	-285	-385	-476	-565	-730	-1876	-1974	-2074	-2177	-2266	-2431
0.2	**0.4**	**0.4**	-70	-47	-70	-39	-146	-247	-2641	-2619	-2641	-2627	-2735	-2836
0.33	**0.33**	**0.33**	197	372	505	594	676	710	-2481	-2305	-2172	-2102	-2020	-1985
0.4	**0.3**	**0.3**	157	326	362	395	307	185	-2497	-2328	-2292	-2277	-2365	-2487
0.6	**0.2**	**0.2**	139	240	255	279	215	120	-2177	-2076	-2061	-2053	-2117	-2212
0.8	**0.1**	**0.1**	73	139	154	158	74	-29	-1484	-1419	-1403	-1410	-1495	-1597
0.9	**0.05**	**0.05**	1607	2755	3587	4181	4789	5090	645	1793	2626	3213	3821	4123

Figure S12 shows some illustrative Brewster Angle Microscopy (BAM) images for the pure and ternary mixtures of DPPC, CHOL, and CCM. The CCM monolayers are very bright even at low surface pressures, which indicates a significant change in the reflection index induced by this monolayer. Interestingly the most stable mixture as indicated by the ΔG_m values at the air water interface ($x_{DPPC}/x_{CHOL}/x_{CCM}$ = 0.4/0.4/0.2) at 30 $mN \cdot m^{-1}$ shows a homogeneous image not as brilliant as it should be accordingly to the CCM fraction, which may be interpreted in terms of a good miscibility of CCM in the DPPC+CHOL mixture.

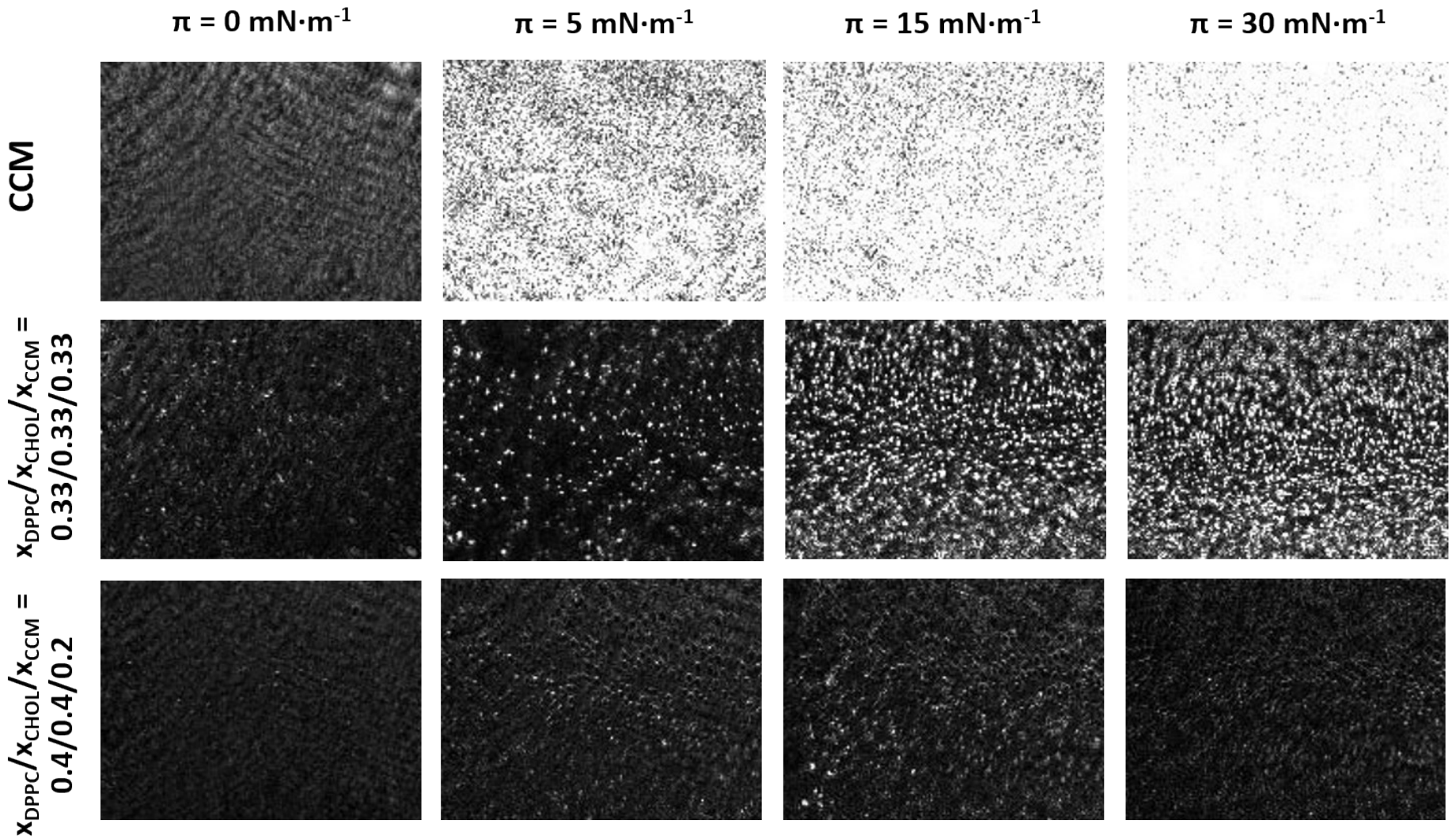

Figure S12. BAM images for pure CCM and the indicated ternary mixtures at several surface pressures. The x-axis is 1860 μm in all images.

Table S.II. Transfer ratios for the pure, binary, and ternary mixtures that were subsequently studied by Atomic Force Microscopy.

System	Transfer ratio
DPPC	1.0
CHOL	1.1
CCM	1.5
DPPC/CHOL x_{DPPC}/x_{CHOL}= 0.5/0.5	1.1
DPPC/CCM x_{DPPC}/x_{CCM}= 0.5/0.5	1.5
CHOL/CCM x_{CHOL}/x_{CCM}= 0.5/0.5	1.3
DPPC/CHOL/CCM $x_{DPPC}/x_{CHOL}/x_{CCM}$= 0.1/0.1/0.8	1.8
DPPC/CHOL/CCM $x_{DPPC}/x_{CHOL}/x_{CCM}$= 0.33/0.33/0.33	1.3
DPPC/CHOL/CCM $x_{DPPC}/x_{CHOL}/x_{CCM}$= 0.4/0.4/0.2	1.2

Transfer ratios higher than 1 account for the instability of the films at the air water interface induced by the CCM.

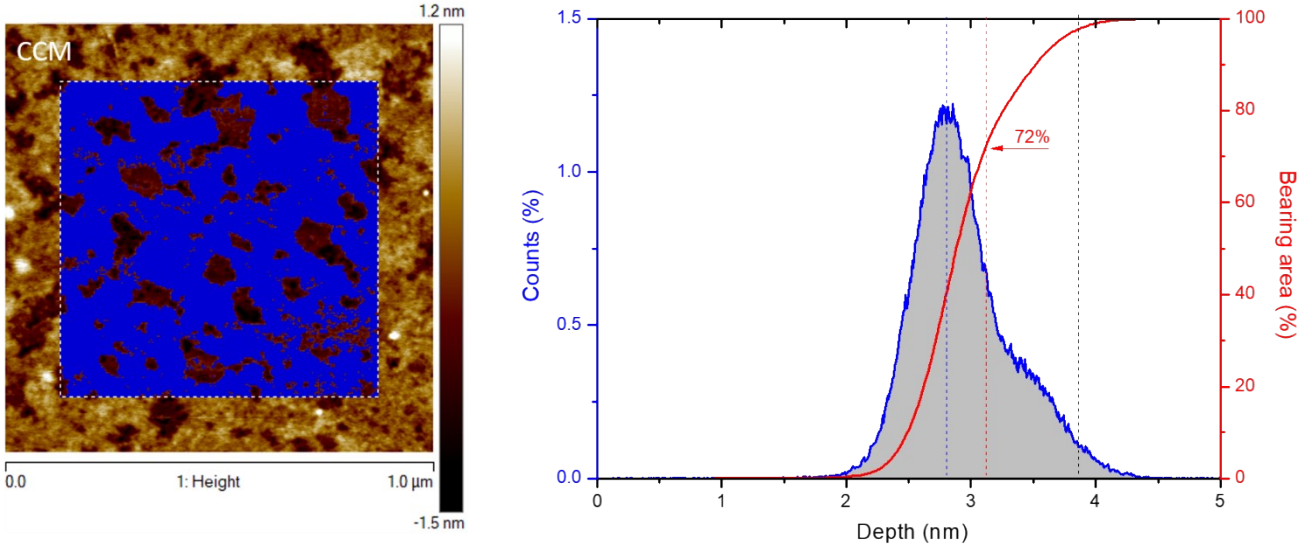

Figure S13. Left: 1 x 1 µm^2 AFM image of a monolayer LB film of CCM with the mask in blue unveiling areas of different height. Right: depth histogram showing the distribution of height data at different depths referred to a reference point, i.e. the highest pixel. The red line (bearing analysis) indicates the relative projected area covered at each depth value depicted as a blue mask in the topographic image corresponding to the white-dashed boxed area in the AFM image. The red arrow accounts for the selected height threshold corresponding to the average height of the measured higher domains.

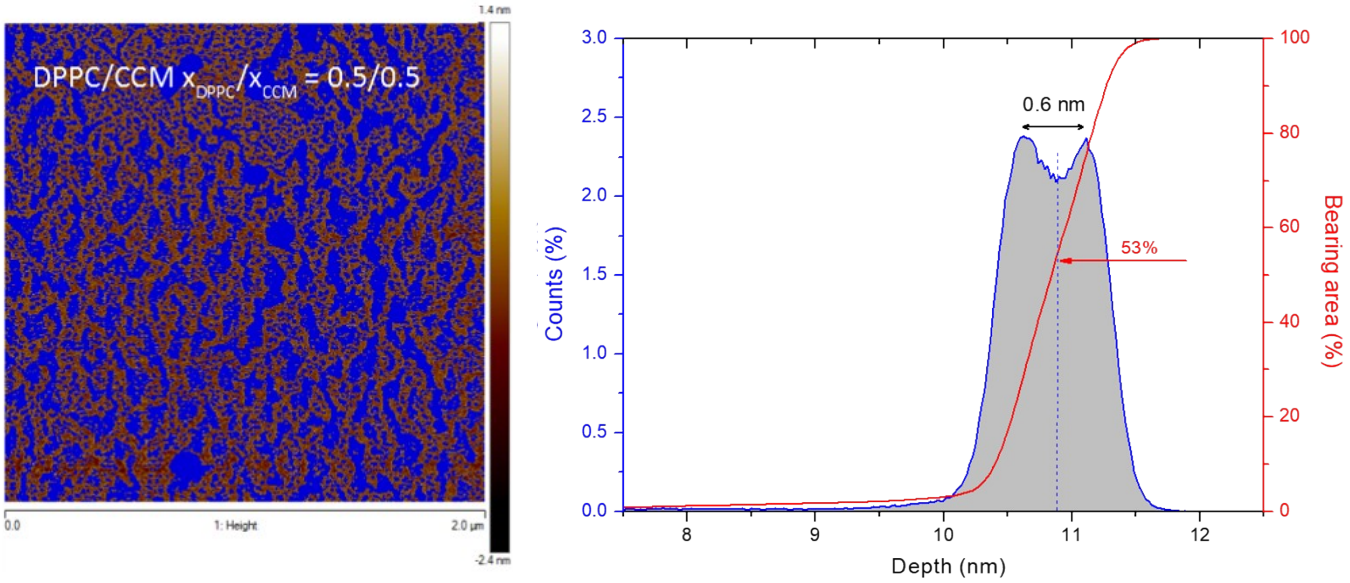

Figure S14. Left: 2 x 2 µm^2 AFM image of a monolayer LB film of DPPC/CCM in a x_{DPPC}/ x_{CCM}= 0.5/0.5 ratio with the mask in blue unveiling areas of different height. Right: depth histogram showing the distribution of height data at different depths referred to a reference point, i.e. the highest pixel. The red line (bearing analysis) indicates the relative projected area covered at each depth value depicted as a blue mask in the topographic image in the AFM image. The red arrow accounts for the selected height threshold corresponding to the average height of the measured higher domains. The average height difference between the two observed domains is 0.6 ± 1 nm.

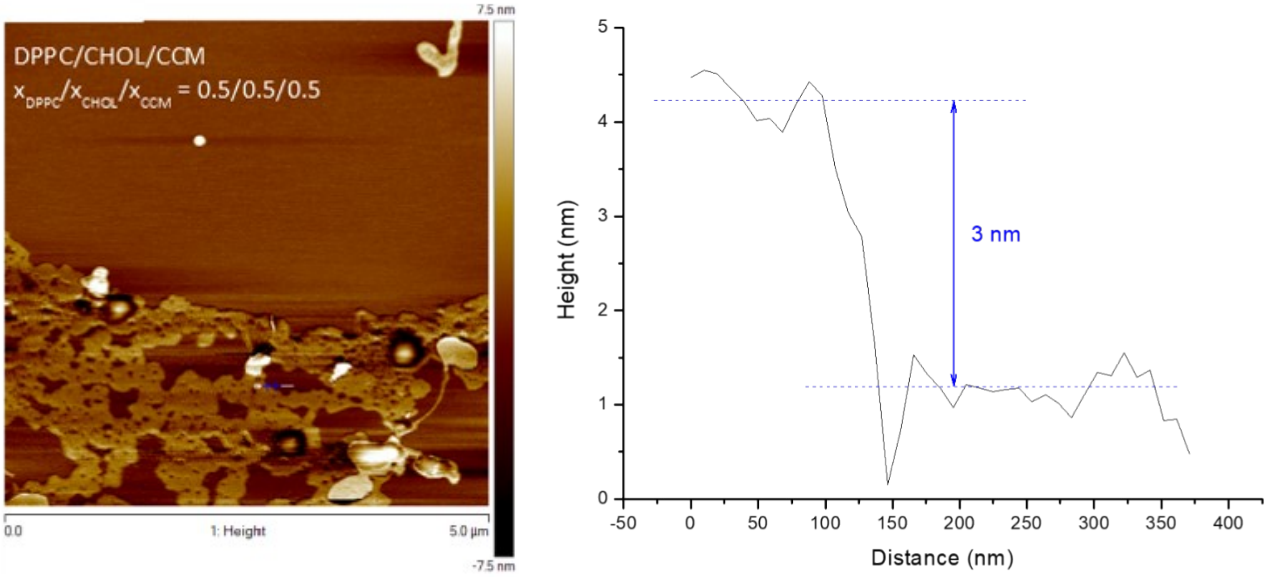

Figure S15. 5 x 5 µm^2 AFM image for a $x_{DPPC}/x_{CHOL}/x_{CCM}$= 0.33/0.33/0.33 LB film transferred at 30 mN·m^{-1} and height profile.

References

(1) Jurak, M. *Thermodynamic Aspects of Cholesterol Effect on Properties of Phospholipid Monolayers: Langmuir and Langmir-Blodgett Monolayer Study.*; *J. Phys. Chem. B.* **2013**, *117*, 3496-3502.

(2) Wydro, P.; Knapczyk, S.; Lapczynska, M. *Variations in the Condensing Effect of Cholesterol on Saturated versus Unsaturated Phosphatidylcholines at Low and High Sterol Concentration.*; *Langmuir* **2011**, *27*, 5433-5444.